2021

Improving the crashworthiness of space frame based vehicles using composites

Nunes, Joseph Nunes

Nunes, E.J. (2021) 'Improving the Crashworthiness of Space Frame Based Vehicles Using Composites', The Plymouth Student Scientist, 14(1), pp. 310-340.
http://hdl.handle.net/10026.1/17329

The Plymouth Student Scientist
University of Plymouth

Improving the crashworthiness of space frame based vehicles using composites

Elliot Joseph Nunes

Project Advisor: Dr Maozhou Meng, School of Engineering, Computing and Mathematics, University of Plymouth, Drake Circus, Plymouth, PL4 8AA

Abstract

This research paper details the investigation into the capability of increasing the crashworthiness of a space frame based vehicle, by the implementation of a modern composite reinforcement technique. This study involves using quasi-static axial compression testing, which is performed on standard structural square and round tubular sample elements of a space frame and specimens of same dimensions which have been reinforced by an exterior cladding of three and five layers of prepreg composite carbon fibre.

Each of these samples are presented in two different lengths of 100mm and 200mm, these lengths are chosen due to being longer and shorter than the critical length of the chosen type of tubing. This is to polarise between local and global buckling and is used to represent longer and shorter structural elements used as part of a space frame, which will undergo global and local buckling failure mode during a collision, respectively.

Results from testing are then used to compare characteristics such as the energy absorbency, specific energy absorbency, maximum load and overall failure mode by processing the force / displacement data derived from the quasi-static compression testing, overall observation of testing and dissection and inspection of tested specimen samples. In addition to real life mechanical testing, FEA and first principle calculations have been utilised to maintain a scientific and critical approach.

Upon analysis of data derived from mechanical testing, it was evident that the composite reinforcement technique played a very large role in increasing energy absorbency and specific energy absorbency of the specimen samples, the most notable being the longer sections which underwent global buckling in their plain, unreinforced state. The composite reinforcement enabled these longer sections to fail in a more desirable local buckling mode, increasing the SEA by up to 703%.

Keywords: space frame, vehicles, crashworthiness, space frame based vehicle, modern composite, reinforcement techniques, energy absorbency, specific energy absorbency, maximum load, overall failure mode, local buckling, global buckling

Introduction

Space frame designs are some of the most common and favoured choice of vehicle chassis types, with vehicles such as the Caterham 7 and Locost kit car being easily assembled and comprised of basic materials such as standard mild steel tubing (Suttie, 2013).

Space frame designs can be advantageous due to their stiffness, if designed appropriately and constructed correctly. Aside from these positives there is a reason why many manufacturers have moved away from space frame designs, which is somewhat due to space frames not being optimised for safety, compared to modern vehicles which have a unibody format. The safety factor in question is that of crashworthiness, modern day vehicle manufacturers incorporate a lot of engineering into making their vehicles perform well during collisions and to applicable industry standards (Nagra, n.d.).

With modern vehicle manufacturers striving for their vehicles to perform increasingly well with crash safety, this technology is more prevalent than ever. Despite the excellent crashworthiness performance of modern cars, space frame based vehicles are still desirable for a multitude of different parties, particularly when it comes to classic vehicles and homebuilt kit cars, such as the Locost which can be homebuilt with a relatively small amount of funds (Webster, 2006). It is for this reason that this study has been performed, to investigate a method of increasing the crashworthiness of these vehicles, with the goal of improving occupant safety.

Project Aims

- The aims of the project will be to investigate and identify the difference in TEA, UCL, SEA and failure mechanism of specimen samples manufactured to represent the space frame of a real vehicle. These characteristics will be examined on tubular structures in their bare form and of the same type that has undergone a composite reinforcement process.

Project Objectives

- Utilise hand calculations done in accordance with ISO 80000 (ISO 80000-1:2009 Quantities and units — Part 1: General, 2009) and FEA software to design and manufacture specimen samples representing tubular components of a vehicle space frame constructed with and without a composite reinforcement technique.
- Perform axial quasi static compression testing on samples and analyse energy TEA, SEA and UCL, using testing guidelines from peer reviewed sources.
- Carry out a comparison of data derived from testing unreinforced and reinforced samples to highlight any improvement in crashworthiness performance.
- Perform visual inspection and analysis of tested samples to investigate failure modes.

Literature Review

The Space Frame Chassis

The specific type of chassis that will be investigated in this project is the space frame **Figure 1**. The space frame chassis utilises round or square section metal tube which is welded together in a triangulated format, allowing for each of the tubular members to either be in compression or tension, each load bearing point must also supported in 3 dimensions (www.formula1-dictionary.net, 2019).

Figure 1: Space Frame Chassis with permission (Clarke, 2009)

The space frame was a desirable format of chassis for cars produced between the 1970s and 1990s with it having the attributes of being light weight and possessing a relatively high level of resistance to torsional forces compared to ladder frame **Figure 2**, or body on frame alternatives (motor-car.net, n.d.). The resistance to torsional forces was due to the triangulated tubular structure of the space frame, mentioned earlier.

Figure 2 - Chris Alston Straight Rail-Frame with permission (Bolig, 2018)

Crash Test Regulations of a Space Frame Chassis Based Vehicle

The space frames manufactured by hobbyists usually have not been tested to conform to any crash test standard, only working to set rules determined by whatever class of racing they are a part of, these rules and regulations generally

determine the metal grade and dimensions. In the case of a Locost amateur race car the chassis tube allowable dimensions are 1 inch square 16swg mild steel tubing (Blackmore and Dorell, 2018).

Moving away from amateur motorsport and focusing on space frame vehicles being built by enthusiasts with the intentions of using them legally on UK roads, this can be done by the individual who has constructed the vehicle applying for a Vehicle Approval through the DVSA. The builder of the car must ensure that their vehicle conforms to the regulations set in the IVA manual for M1 passenger vehicles (www.gov.uk, 2017), none of these regulations however require a crash test of the vehicle.

Turning attention to the manufacturing of space frame-based production cars, vehicles which are produced on a small scale of less than 500 per year are exempt from crash testing analysis via EC legislation (Williams, Pennington and Barton, 2000). Instead of undergoing crash testing, vehicles are instead certified by a third party as conforming to safety regulations, but none of these regulations require a crash test (Weernink, 2005).

Crashworthiness of a Space Frame Chassis in Detail

Crashworthiness is a designed characteristic that has the aim of dissipating energy which is applied to a vehicles during a collision, the desirable outcome is energy being absorbed via ‘crumple zones’ or chassis components that have the purpose of deforming, this results in the occupants of the vehicle experiencing less of the impact energy and an improvement in safety (Mamalis et al., 1998). As a space frame chassis does not generally have the crumple zones that a monocoque chassis would possess, the energy absorbency would take place mostly in the space frame of the vehicle itself. Some of the energy would also be absorbed into the tyres, suspension, and other devices such as radiators and drive line components, depending on the area of the vehicle which the Collison was applied to (Williams, Pennington and Barton, 2000).

The energy absorbency of the framework would be determined by the structural characteristics of the material and size of tubular members used. Chassis components that possessed a high slenderness ratio would be more subject to buckling during forces being applied (www.engineeringcorecourses.com, n.d.) which is one of the reasons behind the additional bracing and reinforcement of longer tubes used as part of a space frame.

Methods of Testing Mechanical Characteristics of Tubular Components

This research paper relies heavily on enlisting a method of testing that is appropriate and would yield the most accurate results, for testing the energy absorbency of a chassis component that is intended to deform during a crash, a high speed crash test rig could be used. This would provide information to determine the deformation behaviour and crashworthiness by projecting a weight of a known value at a set velocity to impact a specific amount of energy onto a specimen (Yoon, Lee and Huh, 2013).

Another method of evaluating crashworthiness and energy absorbency would be to use a drop weight impact tester, this type of machinery can be used to formulate a

load time graph and can determine the energy absorbency of specimens (Taheri-Behrooz, Abdolvand and Shokrieh, 2013).

A simplified method of testing the energy absorbency characteristics, UTS, YS and mechanical failure mechanisms of a specimen is by using the Quasi-static test (White and Jones, 1999). This test method can be performed using a universal test rig, with the only limiting factor being the maximum force capacity of the machine and the 'window' which would determine the maximum physical size of specimens that would undergo testing. In a Quasi-static test a sample is crushed using either an electromechanical or hydraulically propelled crosshead, this is moved at a relatively slow, constant speed which for the axial testing of metal tubes is usually set at a nominal rate of between 2.5mm/min (DiPaolo and Tom, 2006) and 10mm/min (White and Jones, 1999).

The data given from a Quasi-static test is usually presented in a force displacement format and the data can thus be graphed and integrated to determine work done and therefore total energy absorbency. Quasi-static testing is proved to be a suitable low cost and less complex analogue for impact testing and analysing the impact response of structures (L. Weirdie and A. Lagace, 2007). In addition to being employed to determine crashworthiness, Quasi-static compression testing can also be used to analyse other dynamically natured problems such as blast resistance (DiPaolo and Tom, 2006).

Composite Energy Absorbers and Failure Mode Analysis

Composite technology has generally been implemented more quickly in the aerospace industry rather than in the automotive business (Clyne and Hull, 2019), with a lot of focus on replacing heavier metal components with composite equivalents. One area of research which applies to both industries is utilising composites as energy absorption devices, with the idea that a composite structure would achieve a state of conservation of kinetic energy by dissipation into the fibres and matrix of the composite, due to breaches and delamination (Milan et al., 2014).

It is also found to be desirable for the peak failure load of the composite energy absorption device to be kept relatively low, in order to keep forces transmitted to the occupants or vehicle structure, as low as possible (Michele, 2018).

During the process of loading a composite structure in an axial direction to the fibres, the fibres tend to go through a state known as 'micro buckling' due to imperfections such as fibre misalignment during curing. These imperfections begin to initiate the failure of the structure at a certain peak load and it is these failures which play a part in energy absorption. Other failure mechanisms that contribute to the energy absorbency capabilities of a composite are delamination of the layers and fracturing of the fibres (Chambe, Bouvet, Dorival and Ferrero, 2019). One of the most prevalent failure modes of a composite in terms of energy absorbency, however, is found to be the elastic / plastic behaviour of the resin, or matrix (Guimard et al., 2007).

Composite and Metal Hybrid Structures

Although composite energy absorbers generally are designed as purely composite components, methods do exist of combining composite technology with metal structures to provide reinforcement and / or increased energy absorption capability. One of these investigated methods is by the means of an aluminium honeycomb 'fill' of a composite tube, this method has been shown to greatly increase the energy absorbency compared to that of a standard tube, albeit with a decrease in SEA due to the increased weight (Sun *et al*., 2016).Another method which is widely used in the aerospace industry is using a

composite patch repair to reinforce cracked and damaged areas of the metal structure of an aircraft, known as a doubler repair (Baker, Rose and Jones, 2002). Although not strictly designed for energy absorbency the application of a composite doubler, can perform a repair that has exceptional performance under cyclic loading, with the only key preparation being a specific surface finish achieved via an abrasive, for the patch to be bonded to (Baker, Rose and Jones, 2002). This repair process results in a metal-composite hybrid structure, strong enough to withstand the forces that the airframe of an aircraft experiences during flight.

Experimental Process

Outlining Problem and Definition of Specimen Selection and Design

In order for the specimen samples to be manufactured as accurately and true to the real situation as possible, the specifics of the of space frames that would be used to derive data to design the specimen samples for testing were defined, as well as justifying the reasoning behind the choices. Two vehicles were chosen for this purpose.

Vehicle Space Frame 1 – Caterham 7 and Locost Kit Car

The Caterham 7 is a simplistic space frame based sports car which has been designed for track use and to be fully compliant to be driven legally on UK roads.

As this vehicle is classified as being 'low volume' it is provided with exemption for crash testing by EC legislation (Williams, Pennington and Barton, 2000). The Caterham 7 also does not come with any safety features that would be found on a modern car such as stability control or an anti-lock braking system and is not tested by Euro NCAP for crash performance (Caterham Seven review, 2018). This criteria makes the Caterham 7 a vehicle that can be dangerous to drive and more at risk of being involved in a collision.

In addition to the Caterham 7, there exists a very popular derivative of this vehicle, known as the Locost. This is a replica kit car favoured by amateur motorsport enthusiasts who seek the speed and handling of the genuine Caterham 7, without having to pay out for the real article. As the Locost is designed to be home built, several key safety issues are raised, involving the quality of assembly and the materials used to build the space frame, which is usually standard ERW mild steel tubing, of dimensions 25.4mm x 25.4mm 1.6mm WT (Blackmore and Dorell, 2018).

This has vastly different mechanical properties to the A453 high tensile steel tubing of the same dimensions that the modern genuine Caterham 7 frame can be optioned with (Sheehan, 2016). It is therefore justified that the Locost and older Caterham 7

space frames could benefit from an analysis into its crashworthiness performance and a method to improve it.

Vehicle Space Frame 2 – Lamborghini Countach
The Lamborghini Countach is a supercar that first started production in 1974, it was developed and refined in the 1980's to compete with cars from other manufacturers, in the same calibre (Lamborghini Countach LP500S, n.d.). Despite being a vehicle of low production, a prototype of the Countach was crash tested for approval in 1974 by MIRA, based in England (LAMBORGHINI COUNTACH LP500, n.d.).

This testing would have required an acceptable level of safety in that era, however crash testing over the years has increased in strictness obsoleting the older standards. This is proven by many vehicles which were made to an acceptable level of conformance now being considered not as safe, such as many cars manufactured in 2000s likely receiving zero or at most one out of 5 rating in a current NCAP test (Jamieson, 2019). The space frame of this vehicle is mostly comprised of FE360 grade CDS 1.5mm WT steel tube (Santoni, 2015) with a 30mm outside diameter (Pollitt, 2019). The Countach is also a high tier fast road vehicle so is designed to be driven quickly. It is for the above reasons that the Lamborghini Countach space frame has been selected to be the subject of crashworthiness analysis and implementation of a method to potentially improve it.

Specimen Metal Grade and Type Selection Summary
The material and dimensions of the structural components used in the space frame design of the chosen vehicles is summarised in ***Table 1***, using this information specimen samples can be designed as an analogue to represent structural components of the real space frame as closely as possible.

Table 1: Space Frame Tubing Summary by Model

Vehicle	**Frame Tube Material Spec**	**Dimensions**
Caterham 7	Standard ERW mild steel tube	25.4mm square 1.6mm WT
Locost 7	Standard ERW mild steel tube	25.4mm square 1.6mm WT
Lamborghini Countach	FE 360 CDS steel tube	30mm OD round 1.5mm WT

The metal type chosen to use as an analogue for the Caterham 7 and Locost frame structure was E220 grade mild steel **Appendix A** in the exact dimensions shown in ***Table 1***. The metal type chosen to model the structural components for the Lamborghini Countach framework was also E220 grade mild steel, this was chosen as the FE 360 grade of steel tube proved to be difficult to source.

Upon comparison of the datasheets for the FE 360 and E220 grade steel it was visible that the yield strength of the FE 360 steel was 235MPa (**Appendix B**), which was only 6.82% greater than the yield strength of the E220 mild steel (**Appendix A**), so was deemed a suitable equivalent for this experiment. Another slight variance was the OD of the tube, the closest size that was readily available was in an imperial size of 1.25 inches with a 16SWG WT, this converted to a metric size of 31.75mm OD and 1.6mm WT.

Selection and Justification of the Composite Reinforcement Method
The method that has been chosen is inspired by the composite doubler method of reinforcing damaged areas of the airframe of an aircraft by use of a pre prepared composite patch (Baker, Rose and Jones, 2002). The specific method will involve preparing the surface of the tubular specimen and cladding or wrapping the exterior of the tubes with a composite prepreg material to provide reinforcement via the construction of a composite energy absorber around the exterior of the tube. The composite materials that were available to use for this application are summarised in **Table 2**.

Table 2: Comparison of Prepreg Composites (XC110 OUT-OF-AUTOCLAVE COMPONENT PREPREG TECHNICAL DATASHEET, 2017), (MTC510 Epoxy Component Prepreg, 2018).

Manufacturer	**System**	**Resin Weight (%)**	**Compressive Strength 0 (MPa)**	**Compressive Strength 90 (MPa)**	**Autoclave Required**
XPREG	X110 210g 2x2 Twill	42%	483	483	No
SHD Composites	MTC510 C200T 2x2 Twill	42%	615	615	Yes

The material that is used for the composite cladding process is XPREG X110 210g 2x2 Twill has been chosen due to this prepreg system only requiring an oven that is settable to the cure cycle of the composite and not an autoclave. This reduces a lot of set up time that the autoclave would require and allows for multiple specimens to be cured in one oven cycle, improving the quality of the specimen samples by removing potential inconsistencies that multiple cure cycles may introduce. This is because it was possible to fit a whole batch of the same sample type for curing in the oven.

Using the **Equation 1** and composite data from **Appendix C**, calculations were done to determine the thickness of the XPREG composite cladding with ply layers ranging from 1 to 5.

$$t = \frac{\rho_f \cdot V_f}{n \cdot A_f}$$

Inserting values for the XPREG prepreg with 1 layer:

$$t = \frac{(1.8 \times 10^6) \cdot 0.42}{1 \cdot 210} = 0.00027m \; or \; 0.27mm$$

The same formula was then used to calculate the thickness of the cladding for up to 5 plies, summarised in **Table 3**.

Table 3: Composite Cladding Thickness

Number of Layers	1	2	3	4	5
Thickness (mm)	0.27	0.55	0.83	1.11	1.38

With the theoretical thickness of the cladding calculated, it was possible to calculate the cross sectional area of the composite reinforcement element for the square and round tube by using **Equation 2** and **Equation 3** respectively:

$$A_{Composite\ Square} = (Width\ of\ Tube\ (m) + 2 \cdot (Thickness\ of\ laminate\ (m)))^2 - (Width\ of\ Tube(m))^2$$

$$A_{Composite\ Round} = \pi \cdot (Radius\ of\ Tube\ (m) + Thickness\ of\ laminate(m))^2 - \pi \cdot (Radius\ of\ Tube(m))^2$$

Cross sectional area of one layer of composite cladding element applied to 25.4mm square steel tube:

$$\left((25.4 \times 10^{-3}m) + 2 \cdot (2.7 \times 10^{-4}m)\right)^2 - (25.4 \times 10^{-3}m)^2 = 2.77 \times 10^{-5}m^2$$

Cross sectional area of one layer of composite cladding element applied to 31.75mm OD round steel tube:

$$\pi \cdot \left((15.88 \times 10^{-3}m) + (2.7 \times 10^{-4}m)\right)^2 - \pi \cdot (15.88 \times 10^{-3}m)^2 = 2.72 \times 10^{-5}m^2$$

The peak force required to initiate failure of the composite element could then be computed, using the values for cross sectional area of the round and square section composite cladding elements and the composite compressive yield strength (**Appendix C**) and **Equation 4**:

$$F_{Composite\ Element} = \left(\sigma_{Composite\ Element} \cdot A_{Composite\ Element}\right)$$

For one layer of composite cladding applied to 25.4mm square tube:

$$F_{Composite\ Element\ Square} = ((483 \times 10^6 Pa) \cdot (2.77 \times 10^{-5}m^2)) = 13.38 \times 10^3 N$$

For one layer of composite cladding applied to 31.75mm OD round tube:

$$F_{Composite\ Element\ Round} = ((483 \times 10^6 Pa) \cdot (2.72 \times 10^{-5}m^2)) = 13.14 \times 10^3 N$$

The peak force of the plain square and round steel tubing without the composite reinforcement applied could then be found using **Equation 5** using the yield strength of E220 steel and the steel tube cross sectional area:

$$F_{Steel\ Tube} = (\sigma_{Steel\ Tube} \cdot A_{Steel\ Tube})$$

$$F_{Square\ Steel\ Tube} = ((220 \times 10^6) \cdot (1.523 \times 10^{-4})) = 33.51 \times 10^3$$

$$F_{Round\ Steel\ Tube} = \left((220 \times 10^{6}) \cdot (1.515 \times 10^{-4})\right) = 33.31 \times 10^{3}$$

The total peak force of the steel tube combined with the composite cladding could then be found using **Equation 6**:

$$F_{Total} = \left(\sigma_{Composite\ Element} \cdot A_{Composite\ Element}\right) + \left(\sigma_{Steel\ Tube} \cdot A_{Steel\ Tube}\right)$$

This is summarised in **Table 4**.

Table 4: Cladding Cross Sectional Area and Peak Loading

Number of Plies	1	2	3	4	5
25.4mm Square Tube Cross Sectional Area (mm^2)	152.32				
31.75mm Round Tube Cross Sectional Area (mm^2)	151.55				
25.4mm Square Tube Cladding Element Cross Sectional Area (mm^2)	27.72	57.09	87.08	117.70	147.83
31.75mm OD Round Tube Cladding Element Cross Sectional Area (mm^2)	27.15	55.78	84.9	114.53	143.56
Square Tube Cladding Element Peak Force (kN)	13.39	27.57	42.06	56.85	71.4
Round Tube Cladding Element Peak Force (kN)	13.39	26.94	41.01	55.32	69.34
Combined Square Steel Tube and Cladding Element Peak Force (kN)	46.90	61.08	75.57	90.36	104.91
Combined Round Steel Tube and Cladding Element Peak Force (kN)	46.71	60.27	74.33	88.64	102.66

The maximum number of composite layers which was chosen to be used was 5 with the minimum number of layers being 3, these values were chosen as a finite amount of the prepreg was available and a compromise had to be stuck between the effectiveness of the composite reinforcement and the amount of specimen samples that could realistically be produced.

Selecting Lengths of Specimen Samples Using Buckling Study

Both local (axial crushing) and global (lateral displacement) buckling modes can occur during failure of a space frame tubular structure in a collision ***Figure 3***, this is due to the use of long and short tubular components with different length / depth ratios. Specimen samples were designed to model both failure modes to obtain experimental data that was more relevant to real world conditions. A basic study into structural buckling was done to achieve this, with the appropriate calculations done to accurately design the samples and determine two specific lengths, where each mode of failure would take place.

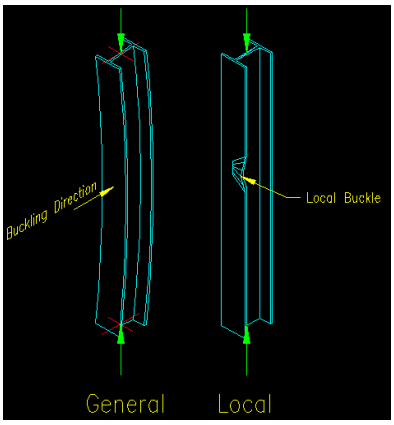

Figure 3: Global vs. Local Buckling (T. Bartlett Quimby, 2014)

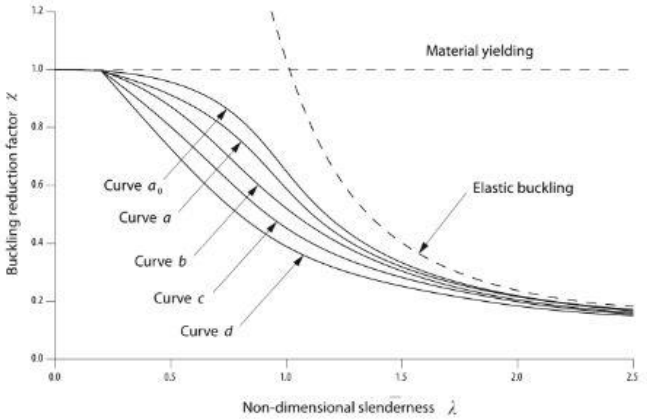

Figure 4: Buckling Reduction Factor vs. Non-Dimensional Slenderness (Stibor, 2014)

To obtain the best result possible, the buckling calculation was done to take the imperfections of the steel tube into account, rather than using the Euler buckling formula shown as the Elastic buckling line in ***Figure 4***. Using the Euler buckling formula alone could potentially overestimate the critical buckling load for compressive force, leading to an inaccurate result.

Resistance to Buckling Calculation

The second moment of area for the square and round section steel tubes was first calculated.

Square tube **Equation 7**:

$$I = \frac{\mathrm{b}_{Outer}\mathrm{h}_{Outer}{}^{3} - b_{Inner}h_{Inner}{}^{3}}{12}$$

$$\frac{(2.54 \times 10^{-2}) \cdot (2.54 \times 10^{-2})^{3} - (2.22 \times 10^{-2}) \cdot (2.22 \times 10^{-2})^{3}}{12} = 1.44 \times 10^{-8}$$

Round Tube **Equation 8:**

$$I = \frac{\pi}{4}({r_{Outer}}^4 - {r_{Inner}}^4)$$

$$\frac{\pi}{4}\left(\left(\frac{31.75 \times 10^{-3}}{2}\right)^4 - \left(\frac{28.55 \times 10^{-3}}{2}\right)^4\right) = 1.73 \cdot 10^{-8}$$

The critical elastic force could then be calculated by substituting the values (I) for the second moment of area into **Equation 9**, as well as the modulus of elasticity of E220 steel (E) and typical lengths of 0.1m and 0.2m, to get the critical elastic force:

$$N_{cr} = \frac{\pi^2 \cdot E \cdot I}{L^2}$$

0.1m square tube:

$$\frac{\pi^2 \cdot (190 \times 10^9) \cdot (1.44 \times 10^{-8})}{0.1^2} = 2700.32 \times 10^3$$

0.2m square tube:

$$\frac{\pi^2 \cdot (190 \times 10^9) \cdot (1.44 \times 10^{-8})}{0.2^2} = 675.08 \times 10^3$$

0.1m round tube:

$$\frac{\pi^2 \cdot (190 \times 10^9) \cdot (1.73 \times 10^{-8})}{0.1^2} = 3244.14 \times 10^3$$

0.2m round tube:

$$\frac{\pi^2 \cdot (190 \times 10^9) \cdot (1.73 \times 10^{-8})}{0.2^2} = 811.03 \times 10^3$$

These N_{CR} values could then be substituted into **Equation 10** to get the slenderness ratio:

$$\lambda = \sqrt{\frac{A \cdot \sigma_y}{N_{cr}}}$$

0.1m square tube:

$$\sqrt{\frac{(1.523 \times 10^{-4}) \cdot (220 \times 10^6)}{(2700.32 \times 10^3)}} = 0.111$$

0.2m square tube:

$$\sqrt{\frac{(1.523 \times 10^{-4}) \cdot (220 \times 10^6)}{(675.08 \times 10^3)}} = 0.223$$

0.1m round tube:

$$\sqrt{\frac{(1.515 \times 10^{-4}) \cdot (220 \times 10^{6})}{(3244.14 \times 10^{3})}} = 0.101$$

0.2m round tube:

$$\sqrt{\frac{(1.515 \times 10^{-4}) \cdot (220 \times 10^{6})}{(808.34 \times 10^{3})}} = 0.203$$

The values for the slenderness ratio (λ) could then be substituted into **Equation 11** to obtain the stability coefficient along with an imperfection factor (α) of 0.49 for cold formed hollow tubing (Member design, n.d.):

$$\phi = 0.5 \cdot [1 + \alpha \cdot (\lambda - 0.2) + \lambda^2]$$

0.1m Square tube:

$$0.5 \cdot [1 + 0.49 \cdot (0.111 - 0.2) + 0.111^2] = 0.484$$

0.2m square tube:

$$0.5 \cdot [1 + 0.49 \cdot (0.223 - 0.2) + 0.223^2] = 0.53$$

0.1m round tube:

$$0.5 \cdot [1 + 0.49 \cdot (0.101 - 0.2) + 0.101^2] = 0.478$$

0.2m round tube:

$$0.5 \cdot [1 + 0.49 \cdot (0.203 - 0.2) + 0.203^2] = 0.521$$

The values for the stability coefficient (ϕ) and the slenderness ratio (λ) could then be substituted into **Equation 12** to obtain the buckling curve reduction factor for each specimen:

$$\chi = \frac{1}{\phi + \sqrt{\phi^2 - \lambda^2}}$$

0.1m square tube:

$$\frac{1}{0.484 + \sqrt{0.484^2 - 0.111^2}} = 1.047$$

0.2m square tube:

$$\frac{1}{0.53 + \sqrt{0.53^2 - 0.223^2}} = 0.989$$

0.1m round tube:

$$\frac{1}{0.478 + \sqrt{0.478^2 - 0.101^2}} = 1.058$$

0.2m round tube:

$$\frac{1}{0.521 + \sqrt{0.521^2 - 0.203^2}} = 0.999$$

Finally, the values for the stability coefficient (χ), cross sectional area of tube (A), yield strength of E220 steel (σ_y) and partial resistance factor for buckling (γ) found to be 1.00 for buckling resistance (Member design, n.d.), can be substituted into **Equation 13** to find resistance force to buckling, corrected for imperfections:

$$N_{ca} = \frac{\chi \cdot A \cdot \sigma_y}{\gamma}$$

0.1m square tube:

$$\frac{1.047 \cdot (1.523 \times 10^{-4}) \cdot (220 \times 10^6)}{1.00} = 35.08 \times 10^3$$

0.2m square tube:

$$\frac{0.989 \cdot (1.523 \times 10^{-4}) \cdot (220 \times 10^6)}{1.00} = 33.14 \times 10^3$$

0.1m round tube:

$$\frac{1.058 \cdot (1.515 \times 10^{-4}) \cdot (220 \times 10^6)}{1.00} = 35.26 \times 10^3$$

0.2m round tube:

$$\frac{0.999 \cdot (1.515 \times 10^{-4}) \cdot (220 \times 10^6)}{1.00} = 33.30 \times 10^3$$

Comparison of Calculated Buckling Force with Nominal Point Loading

Table 5: Comparison of 0.1m and 0.2m Length Tubes for Buckling Likelihood

Specimen Type	Nominal Failure Force (kN)	Critical Buckling Load (kN)	Percentage Difference	Likely to Buckle
0.1m Square Tube	33.51	35.08	-4.69%	No
0.2m Square Tube	33.51	33.14	1.1%	Yes
0.1m Round Tube	33.32	35.26	-5.82%	No
0.2m Round Tube	33.32	33.30	0.0006%	Yes

Observing ***Table 5*** it is visible to see that the square and round tubes that have lengths of 0.2m will reach the critical buckling load before the nominal failure force, this indicates that these sections will undergo global buckling, rather than failure by crushing.

SolidWorks FEA Buckling Study

SolidWorks CAD and FEA software were used to generate computer models in the dimensions of the round and square tubular specimens, to critique and confirm the numerical calculations which were used to select the lengths of tubular samples in **section 6.1.5**. The axial compressive forces were set up to model the critical buckling forces shown in ***Table 5*** for each of the 4 specimens ***Figure 5***. The material properties were customised to represent the E220 grade of steel **Appendix A** and a high quality mesh with 22736 elements was used to yield a high accuracy result.

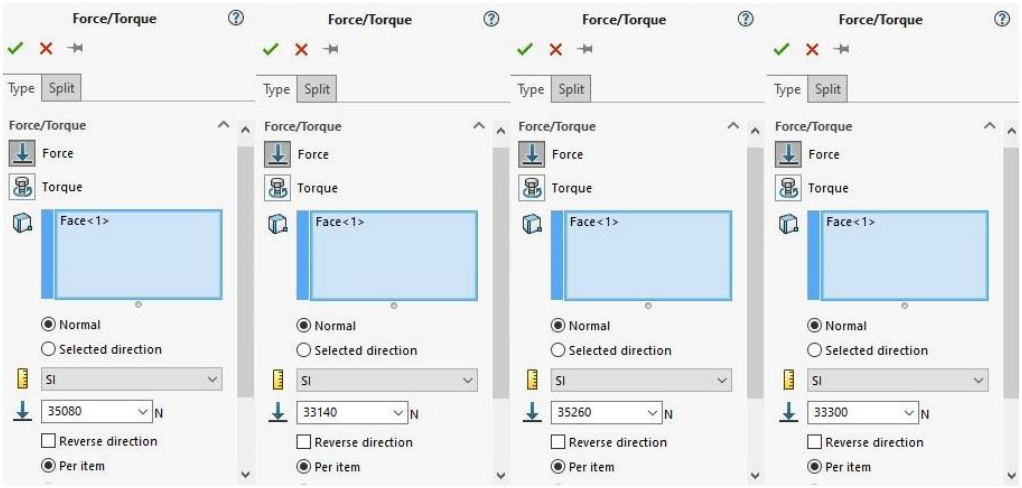

Figure 5: Axial Compressive Force Values

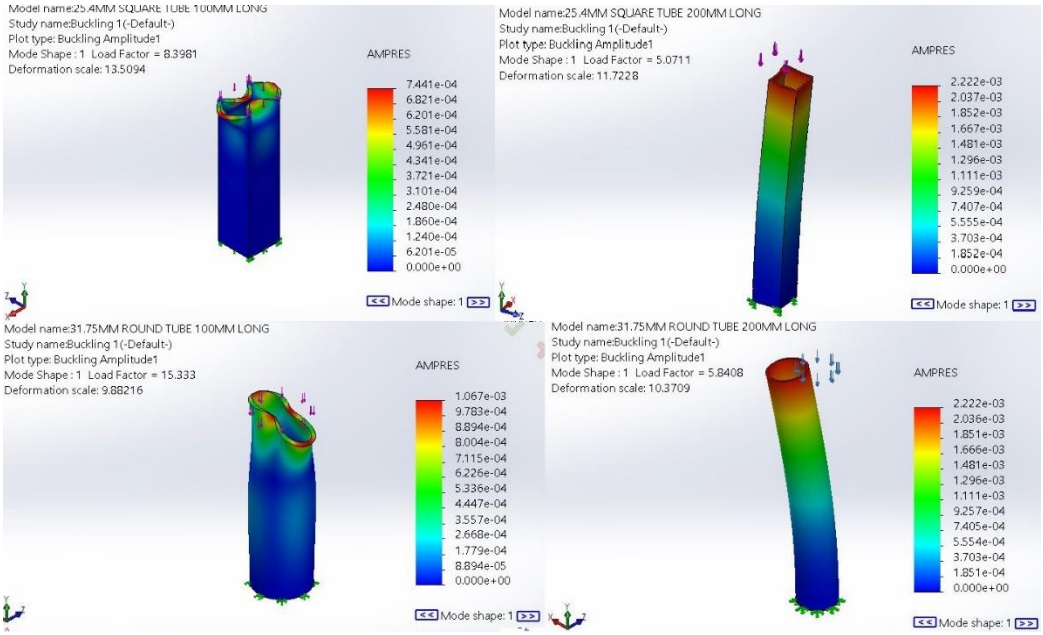

Figure 6: Local vs. Global Buckling of 100mm and 200mm Long Samples

Figure 6 shows a side by side comparison of the buckling failure modes for both lengths of specimen sample, 100mm on the left and 200mm on the right. It is visible that the computer model confirms that the tubes of 100mm length buckle in a local mode and the 200mm length tubes buckle in a global mode, therefore adding further evidence to prove that both buckling modes could be modelled in a real life scenario by using these specific lengths.

Manufacture of Specimen Samples

Manufacturing began by collating all the applicable risk assessments, these were the assessment for working with epoxy prepreg materials **Appendix D**, cutting dry fabric in the composites lab **Appendix E** and the assessment for using the abrasive saw for cutting specimen samples **Appendix F**. These assessments were carefully reviewed and followed to ensure safety of working practices. All specimen samples were manufactured in line with the requirements of the test matrix **Appendix G**.

The unreinforced square and round section specimens were prepared by first cutting the supplied 3 meter lengths of round and square E220 steel tube stock into manageable lengths with a hacksaw **Figure *7.*** The shorter lengths were then cut accurately into 100mm and 200mm lengths using the Abrasimet cut-off saw ***Figure 8***, care was taken to apply light cutting pressure as to not heat up the metal excessively. The cut samples were then lightly deburred using a half round file ***Figure 9***. This process was repeated until all the unreinforced steel specimens were constructed, (specimen idents P100S1, P200S1, P100R1 and P200R1).

Figure 7: Cutting Steel Stock to Length

Figure 8: Using Abrasimet Cut-Off Saw for Accuracy

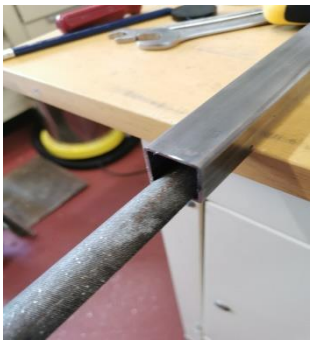

Figure 9: Deburring Tube

Figure 10: Degreasing Steel Stock

Figure 11: Tube Cut Length in Blasting Cabinet

Figure 12: Media Blasted E220 Steel Tube

The composite prepreg reinforced specimens were prepared by first applying a degreasing agent to the steel stock ***Figure 10***, to prepare the tubing for media blasting. The tubes were then cut into shorter lengths, so it was possible to fit them into the media blasting cabinet ***Figure 11***. The exterior of the tube was then blasted with 30 grit media ***Figure 12*** which was done to obtain an optimum surface finish for bonding with the prepreg composite (Islam, Tong and Falzon, 2014).

After blasting had concluded the prepared surface of the steel tubing was cleaned to remove debris left from blasting, before the prepreg composite could be applied. The XPREG XC110 210g was then removed from the freezer and left to thaw, when it was ready for use it was wrapped tightly around the prepared steel tubes with the with the prepreg orientation at 0 degrees to the axis of the steel tube ***Figure 13***.

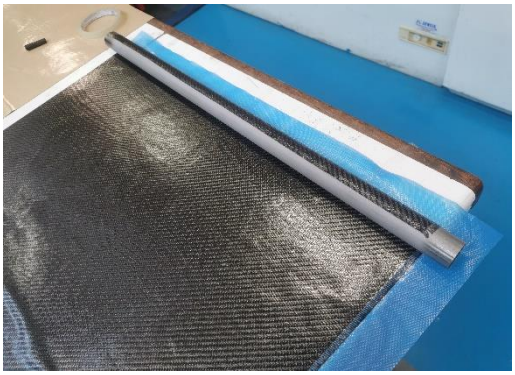

Figure 13: Application of XPREG XC110 Prepreg to Round Tube

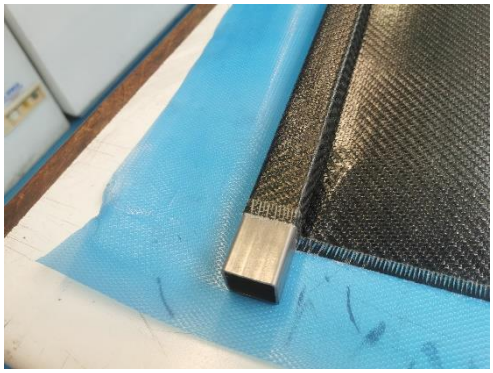

Figure 14: Application of XPREG XC110 Prepreg to Square Tube

The steel tubes were wrapped with either 3 or 5 layers of prepreg, depending on the specimen sample type that was being constructed. After the prepreg had been applied, a layer of polyester peel ply fabric was added, with a layer of perforated release film covering the peel ply layer ***Figure 15***. The final step was applying a breather layer cloth to allow for a vacuum to be applied to all of the samples uniformly to aid in bonding of layers and vacuum bagging which was done by 'chain linking' all the samples together so they could be oven cured ***Figure 16***. The specific cure cycle provided by the manufacturer of the prepreg **Appendix C** was used to cure the prepreg for optimum performance and strength.

Figure 15: Application of Peel Ply and Release Film

Figure 16: 'Chain Linked' Prepreg Wrapped Tubes in Vacuum Bag

After curing, the composite clad steel tubes were unwrapped and accurately sectioned into 100mm and 200mm lengths ***Figure 17***. Each sample was clearly labelled with an identifier ***Figure 18*** and weights tabulated for later calculation of SEA **Appendix H**.

Figure 17: Composite Clad Steel Tubes Cut to Length

Figure 18: Composite Clad Specimen Samples Weighed and Labelled

Design and Manufacture of Centring Bosses

In addition to the design and construction of the specimen samples, adapters had to be made which would allow for the tubular specimens to be mounted into the universal testing machine. The adapters were designed in SolidWorks and made to securely hold the square and round tube specimens during the compression testing **Appendix I** and **Appendix J**. Manufacturing was done by the technicians in the Brunel workshop, a request form which was signed by the project adviser had to be generated in order to allow for the manufacturing to take place **Appendix K**.

Figure 19: Universal Testing Machine Adapters

Figure 20: Adapters Fitted to Specimen

Specimen Sample Testing

Test matrix **Appendix G** was used to manage testing of specimen samples and directly reference the ident labels applied during manufacture of specimens ***Figure 18***. Two of each type of specimen sample was tested to compute an average of the two tests and yield data of more accuracy. Each specimen sample was secured into the universal testing machine by use of the appropriate type of centring bosses depending on whether round or square section samples were being tested.

The universal testing machine was programmed to perform a compression test with a crosshead speed of 3mm/min, a speed well within the range for a standard quasi-static compression test with the minimum usually being set between 3mm/min (DiPaolo and Tom, 2006) and the maximum value being 10mm/min (White and Jones, 1999). The final displacement of the test was set at 50% for each specimen, however the test would be manually stopped before this range was reached if a specimen were globally buckling ***Figure 21***, this was to prevent samples being ejected from the machine.

If specimen samples exhibited axial crushing in a local buckling mode ***Figure 22***, the full displacement would be allowable. Before every test, the machine was calibrated and balanced to ensure maximum accuracy of data gathering.

Figure 21: Global Buckling

Figure 22: Local Buckling

The raw data from the compression test of each specimen was output in the format of an Excel document. This data detailed a value for time in seconds, displacement in mm and force in kN **Appendix L**. The raw data values for the force and displacement were put together and presented in a graph for a clearer analysis and to get a visual representation of how the specimen sample failed, to find the applicable buckling mode.

To determine the TEA of each sample, principles from **Equation 14** were used, this would usually involve an integration operation of the whole area underneath the force displacement curve to calculate work done, or specifically in this case TEA.

As the data was contained within Excel there was no facility for integration, therefore a method known as ‘rectangular integration’ (Cai, 2014) was used to effectively ‘slice’ the area under the curve into thin sections and sum them together to approximate the total area, this yielded a value that was accurate enough to be used for the purpose of calculating energy absorbency with a negligible effect on accuracy compared to performing actual numerical integration. This process is however a fundamental theory of the method of integration.

With the TEA calculated, the SEA could then be determined by inserting the value for the TEA and the weight of the specimen sample into **Equation 15**, this enables the generation of a universal value which can be used to compare the performance of all the specimen samples.

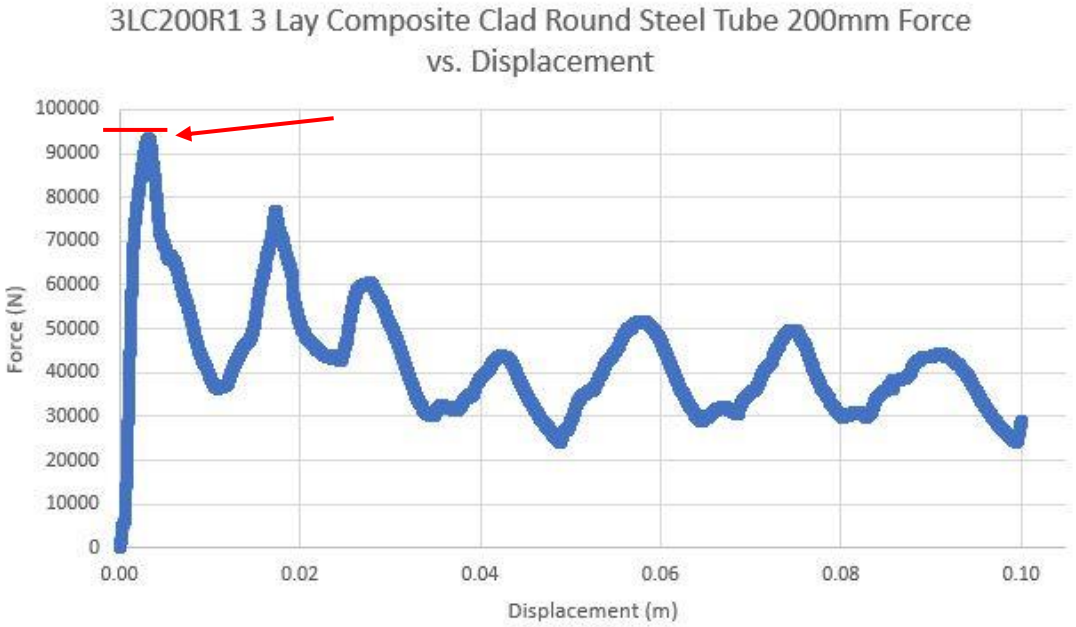

Figure 23: UCL From Force Displacement Graph

In addition to the TEA, the UCL could be derived from the raw data, using the highest force value displayed, this occurred during the first peak of the force displacement curve ***Figure 23***. This was an important value as it played a part in determining the crashworthiness suitability of the specimen sample.

Results

The test data was first presented in four separate groups **Appendix M**. the UCL, TEA and SEA were presented on the tables as well as the percentage difference of each value between unreinforced steel tube samples and of composite reinforced steel tube specimens to identify any changes. Average values of the UCL, TEA, SEA and percentage differences were then computed from the two tables of the same set i.e. 3LC200S1 (set 1) and 3LC200S2 (set 2) and tabulated **Appendix N**, this was done to present a better level of accuracy.

A brief review of the 100mm length specimens show the composite cladding reinforcement allowed for a higher level of TEA across the board when compared to the TEA of unreinforced tubes. Despite the composite cladded specimens being marginally heavier when compared to unreinforced specimens, the SEA of the composite reinforced specimens was also higher than that of unreinforced samples in nearly every case, this was because despite the cladding adding weight, the increase in TEA was significant allowing for a higher SEA value.

Figure 24 displays a comparison between the UCL and SEA of the shorter 100mm round and square specimen samples. These two factors are critical for a crashworthiness application with the desirable format being a high SEA with a low UCL.

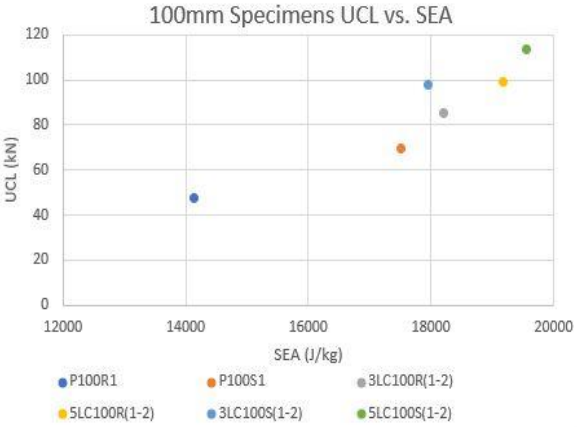

Figure 24: UCL vs. SEA 100mm Specimens

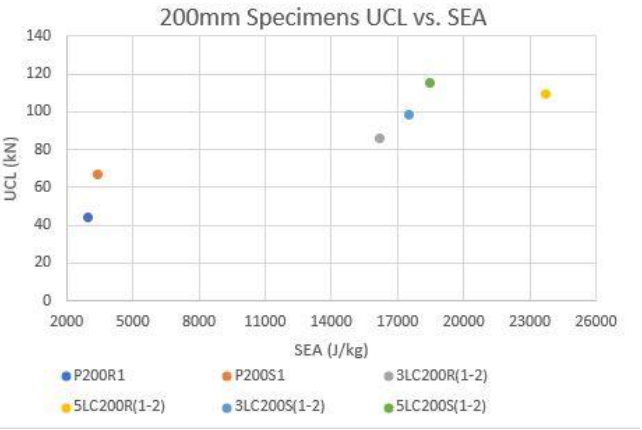

Figure 25: UCL vs. SEA 200mm Specimens

There is a clear correlation between the samples with more layers of composite having a higher UCL, with specimens 5LC100S(1-2) and 5LC100R(1-2) having the highest peak loading of 113.85kN and 109.55kN. This is caused by the composite cladding being more resistant to crushing with more layers being used, displayed in ***Table 4***.

The specimen sample that proved to be the most promising in this group was sample 3LC100R(1-2), which showed a substantial increase in SEA of 28.83%, but had the lowest value of UCL for all the reinforced samples tested at 85.34kN . This sample was also desirable from an economic perspective, requiring the minimum number of composite layers (3) of the samples tested.

Figure 26: Global Buckling of 200mm Specimen P200R1

Figure 27: Local Buckling of 200mm Reinforced Specimen 3LC200R1

The specimen samples that showed the most notable improvements overall were the 200mm length samples visible in ***Figure 25***. The composite reinforcement applied to tubes of this length provided a constraining property which prevented the longer samples from buckling globally ***Figure 26*** and only achieving a maximum possible displacement of 25mm. The 200mm length composite reinforced samples exhibited a local buckling mode, allowing them to reach the full 100mm displacement **Figure 27**, aiding in increased energy absorbency. This appeared to be caused by the composite progressively failing along the length of the tube, effectively decreasing the critical length.

The energy absorbency increase due to the change in buckling mode of the longer samples increased the SEA of the 5LC200R(1-2) samples by up to 703.33% and the 5LC200S(1-2) samples by up to 444.63% when compared to the SEA samples P200R1 and P200S1. Similar in the case of the shorter 100mm samples that had 5 layers of cladding, this increase in SEA came with the expense of having an undesirable higher UCL.

The sample which displayed the best overall crashworthiness characteristics in this group was 3LC200R(1-2), this sample had 3 layers of composite reinforcement and yielded a greater increase in SEA than sample 5LC200S(1-2) that had 5 layers, it also had a lower increase in UCL compared to the other samples at 85.64kN. This was another specimen that was also economically viable as it only required 3 layers of composite reinforcement to achieve a good level of improvement.

Visual Examination and Assessment of Specimens

With the testing concluded, an examination was done to gain a deeper understanding into the performance of the composite cladding reinforcement and provide more evidence to support its effectiveness. The samples which were deemed to perform the best from testing, 3LC100R2 and 3LC200R2 from the averaged groups were sectioned to investigate how the specimen failed ***Figure 28***.

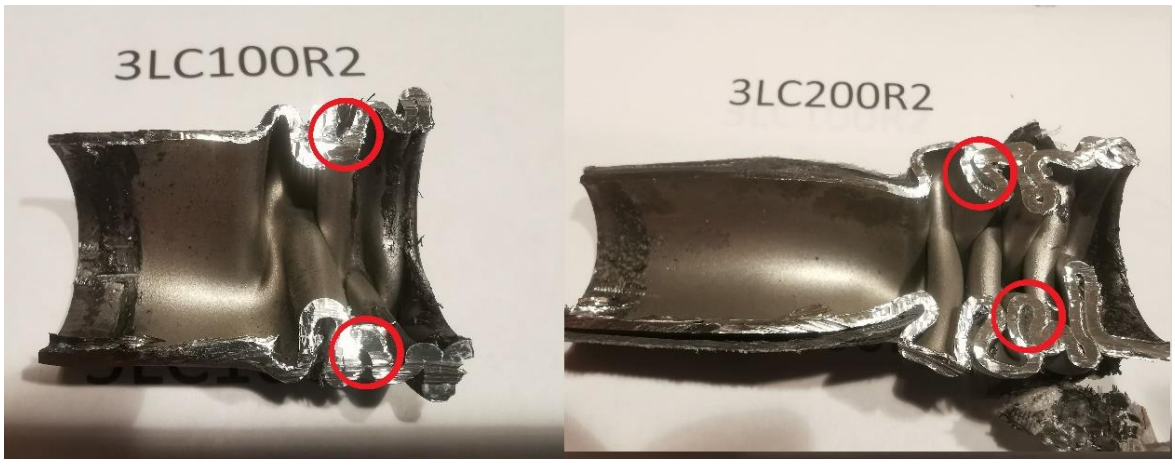

Figure 28: Visual Failure Analysis

With an interior view it was possible to see that the composite reinforcement remained bonded to the surface of the steel tube, as it was still present within the locally buckled layers of the steel. The failure mechanism of the composite

reinforcement was via delamination of the layers within the reinforcement leading to the conclusion that the composite itself provided a means of absorbing a lot more energy than the plain tube would have been able to.

A financial analysis ***Table 6*** also provided evidence to suggest that the composite reinforcement method is an economically viable option, with minimal material costs required to achieve a substantial increase in SEA and crashworthiness.

Table 6: Composite Reinforcement Cost Analysis

Specimen Type	**Composite Required m^2**	**Composite Reinforcement Cost £**	**SEA Improvement Cost (£/J/kg)**
3LC100S(1-2)	0.0305	1.30	0.00295
3LC100R(1-2)	0.0299	1.27	0.000313
5LC100S(1-2)	0.0508	2.17	0.00106
5LC100R(1-2)	0.0498	2.12	0.000423
3LC200S(1-2)	0.0610	2.60	0.000184
3LC200R(1-2)	0.0598	2.55	0.000192
5LC200S(1-2)	0.1016	4.33	0.000288
5LC200R(1-2)	0.0997	4.25	0.000204

Cost of Composite (£/m^2)	42.62

Conclusions

The project ran very smoothly, despite some minor setbacks which resulted in some of the desired testing such as transverse bend and fatigue having to be phased out due to equipment unavailability. The aims and objectives of the project were mostly met starting with the detailed the detailed theoretical analysis for the design of the samples, this was done to the best standard possible and resulted in a set of well-designed specimen samples being produced for testing with a justification made for each of the design aspects, eliminating any ambiguity.

The testing was done to the standards that were originally set out, with clear values defined for the TEA, SEA and UCL of all specimen samples and with no major problems occurring. This resulted in a set of accurate data being produced which was then critiqued and presented in order to carry out a comparison and define the specimen samples that had the best performance, therefore indicating the optimum format for the composite cladding method.

A visual inspection was also done to further investigate failure modes by section cutting tested samples, this provided valuable information into the performance of the composite reinforcement process, allowing for the specimen design to be improved even further in the future. Overall, the project was deemed a success, with clear evidence supporting that the composite reinforcement method played a large role in the improvement of crashworthiness characteristics of structural components of a space frame chassis.

Recommendations

If this project were to be continued or taken to further levels of detail, one of the first steps would be to perform dynamic impact testing, this test method was not chosen for the project this far due to its complexity and associated costs but would allow for a greater understanding into how the composite clad specimens would behave during a high speed impact.

Given more time and resources available more variants of specimen samples could be created. This could involve a better variance of composite layers instead of just the 3 and 5 layer specimens that were used in this project. The result of this could be fine tuning the performance of the cladding and seeking the optimum configuration to decrease UCL whilst increasing the SEA. A greater variety of specimen samples could also include testing samples longer than 200mm to investigate buckling modes at greater lengths.

The final recommendation is the minimisation of costs, time and resources as much as possible, an example of which is tuning of the universal testing machine crosshead speed whilst still staying within the bounds of a quasi-static test, a faster speed results in tests being performed more quickly.

Acknowledgements

Firstly, I would like to thank the staff who assisted in the first lot of mechanical testing that was carried out in the Smeaton laboratory, Mr Terry Richards and Dr Jeremy Clark. I would also like to extend thanks to my supervisor Dr Maozhou Meng who gave me guidance to keep my project on track and provide advice where needed and my project moderator Mike Miles, who provided constructive feedback in order to identify areas of my project to improve on and expand my knowledge to make it as high quality as possible.

My gratitude is also given to Dr Long Yuan Li who helped with the structural element of my project and Dr Richard Cullen who assisted with the manufacturing of the composite element of my project.

I would also like to thank Iain Jack and his team at Metaltest UK who provided all the mechanical testing I required, due to the universities Smeaton lab being closed and unavailable to use because of the Covid-19 situation. This enabled me to continue my project without having to remove its practical elements and still achieve the best outcome possible.

Finally, I would like to thank my family who have been here to support me endlessly through not only this project but my whole university career, especially my one year old daughter, Elia who has been a continuous source of motivation to progress and succeed, even when the mixture between parenting, working and university got tough.

Nomenclature

Symbol	**Quantity**	**SI Units - Value**
A	Area	m^2
SEA	Specific Energy Absorbency	J/kg
σ	Stress	N/m^2
ε	Strain	Unitless
J	Joule	N·m
E	Youngs Modulus	N/m^2
W	Work Done	N·m
L	Length	m
λ	Slenderness Ratio (sections of class 1, 2 and 3)	Unitless
α	Imperfection Factor	Unitless – 0.49
χ	Buckling Curve Reduction Factor	Unitless
Φ	Stability Coefficient	Unitless
A_f	Area Weight of Composite Fabric	kg/m^2
ρ_f	Fibre Density	kg/m^3
V_f	Volume Fraction of Composite	Unitless
t	Laminate Thickness	m
n	Number of Composite Ply Layers	Unitless
F	Force	N
ΔL	Change in Length	m
TEA	Total Energy Absorbency	N·m
I	Moment of Inertia	kg·m^2
γ	Partial Resistance Factor for Buckling	Unitless – 1.00
σ_y	Material Yield Strength	Pascals
GSM	Grams per Square Meter	kg/m^2
N_{CR}	Resistance to Buckling	N
UCL	Ultimate Compressive Load	N
YS	Yield Strength	Pa
Acronym	**Meaning**	
ERW	Electrically Resistance Welded	
CDS	Cold Drawn Seamless	
WT	Wall Thickness	
OD	Outside Diameter	
SWG	Standard Wire Gauge	

List of Formulas

(1) Laminate Thickness

$$t = \frac{n \cdot A_f}{\rho_f \cdot V_f}$$

(2) Cross Sectional Area of Square Tube Composite Cladding

$$A_{Composite\ Square} = \big(Width\ of\ Tube + 2 \cdot (Thickness\ of\ laminate)\big)^2 - (Width\ of\ Tube)^2$$

(3) Cross Sectional Area of Round Tube Composite Cladding

$$A_{Composite\ Round} = \pi \cdot (Radius\ of\ Tube\ (m) + Thickness\ of\ laminate(m))^2 - \pi \cdot (Radius\ of\ Tube(m))^2$$

(4) Peak Load of Composite Cladding Element

$$F_{Composite\ Element} = \big(\sigma_{Composite\ Element} \cdot A_{Composite\ Element}\big)$$

(5) Peak Load of Steel Tube

$$F_{Steel\ Tube} = (\sigma_{Steel\ Tube} \cdot A_{Steel\ Tube})$$

(6) Peak Load of Composite Reinforced Steel Tube

$$F_{Total} = \big(\sigma_{Composite\ Element} \cdot A_{Composite\ Element}\big) + (\sigma_{Steel\ Tube} \cdot A_{Steel\ Tube})$$

(7) Moment of Inertia for Hollow Square Section

$$I = \frac{\mathrm{b}_{Outer}\mathrm{h}_{Outer}{}^3 - b_{Inner}h_{Inner}{}^3}{12}$$

(8) Moment of Inertia for Hollow Round Section

$$I = \frac{\pi}{4}(r_{Outer}{}^4 - r_{Inner}{}^4)$$

(9) Critical Elastic Force

$$N_{cr} = \frac{\pi^2 \cdot E \cdot I}{L^2}$$

(10) Slenderness Ratio

$$\lambda = \sqrt{\frac{A \cdot \sigma_y}{N_{cr}}}$$

(11) Stability Coefficient

$$\phi = 0.5 \cdot [1 + \alpha \cdot (\lambda - 0.2) + \lambda^2]$$

(12) Buckling Curve Reduction Factor

$$\chi = \frac{1}{\phi + \sqrt{\phi^2 - \lambda^2}}$$

(13) Resistance to Buckling

$$N_{ca} = \frac{\chi \cdot A \cdot \sigma_y}{\gamma}$$

(14) Total Energy Absorbency

$$TEA = \int F(x)\, dx$$

(15) Specific Energy Absorbency

$$SEA = \frac{TEA}{Weight\ of\ Specimen} = \frac{J}{kg}$$

References

adrianflux.co.uk. n.d. Lamborghini Countach LP500S. [online] Available at: <https://www.adrianflux.co.uk/supercars/lamborghini-countach/> [Accessed 10 April 2020].

autoexpress.co.uk. 2018. Caterham Seven Review. [online] Available at: <https://www.autoexpress.co.uk/caterham/7> [Accessed 10 April 2020].

Baker, A., Rose, L. and Jones, R., 2002. *Advances In The Bonded Composite Repair Of Metallic Aircraft Structure*. 1st ed. Oxford: ELSEVIER SCIENCE LTd, p.9, 485.

bebonchina.com. n.d. Fe 360 CK1 Chemical Composition, Fe 360 CK1 Mechanical Properties. [online] Available at: <http://www.bebonchina.com/Selling-list/Fe-360-CK1-Chemical-composition-Fe-360-CK1-Mechanical-properties.html> [Accessed 16 April 2020].

Blackmore, R. and Dorell, A. (2018). Locost Championship Sporting & Technical Regulations 2019. [ebook] 750 Motor Club Ltd, p.4. Available at: https://www.750mc.co.uk/formulae/750-formula/regulations.htm [Accessed 10 April. 2020].

Bolig, R. (2018). Chris Alston Straight-Rail Frame. [image] Available at: https://www.turnology.com/news/chassisworks-new-frames/ [Accessed 10 April. 2020].

Cai, E., 2014. Rectangular Integration (A.K.A. The Midpoint Rule) – Conceptual Foundations And A Statistical Application In R. [online] chemicalstatistician.wordpress.com. Available at: <https://chemicalstatistician.wordpress.com/2014/01/20/rectangular-integration-a-k-a-the-midpoint-rule/> [Accessed 21 April 2020].

Chambe, J., Bouvet, C., Dorival, O. and Ferrero, J., 2019. Energy absorption capacity of composite thin-wall circular tubes under axial crushing with different trigger initiations. Journal of Composite Materials, [online] 54(10), p.1. Available at: <https://www.researchgate.net/publication/336043778_Energy_absorption_capacity_of_composite_thin-wall_circular_tubes_under_axial_crushing_with_different_trigger_initiations> [Accessed 10 April 2020].

Clyne, T. and Hull, D. (2019). An Introduction to Composite Materials. 3rd ed. Cambridge: Cambridge University Press, p.323.

DiPaolo, B. and Tom, J., 2006. A study on an axial crush configuration response of thin-wall, steel box components: The quasi-static experiments. International Journal of Solids and Structures, [online] 43(0020-7683), pp.7755, 7764. Available at: <https://www.sciencedirect.com/science/article/pii/S0020768306001016> [Accessed 10 April 2020].

easycomposites.co.uk. 2017. XC110 OUT-OF-AUTOCLAVE COMPONENT PREPREG TECHNICAL DATASHEET. [online] Available at: <https://3937524.app.netsuite.com/core/media/media.nl?id=150680&c=3937524&h=8ce3f5fc4e9e2a09ec25&_xt=.pdf> [Accessed 16 April 2020].

engineeringcorecourses.com. (n.d.). C5.1 Euler's Buckling Formula. [online] Available at: http://www.engineeringcorecourses.com/solidmechanics2/C5-buckling/C5.1-eulers-buckling-formula/theory/ [Accessed 10 April. 2020].

formula1-dictionary.net. (n.d.). Chassis explained. [online] Available at: http://www.formula1-dictionary.net/chassis.html [Accessed 10 April. 2020].

gov.uk. (2017). Individual Vehicle Approval (IVA) for cars: help to get a pass. [online] Available at: https://www.gov.uk/government/publications/individual-vehicle-approval-iva-for-cars-help-to-get-a-pass/individual-vehicle-approval-iva-for-cars-help-to-get-a-pass [Accessed 10 April. 2020].

Guimard, J., Allix, O., Pechnik, N. and Thevenet, P. (2007). Statistical Energy and Failure Analysis of a CFRP Compression Behaviour Using a Uniaxial Microbuckling Model. Journal of Composite Materials, [online] 41(0021-9983), pp.2807, 2827. Available at: https://journals.sagepub.com/doi/10.1177/0021998307079980 [Accessed 10 April. 2020].

Islam, M., Tong, L. and Falzon, P., 2014. Influence of metal surface preparation on its surface profile, contact angle, surface energy and adhesion with glass fibre prepreg. International Journal of Adhesion and Adhesives, [online] 51(2014), p.40. Available at: <https://www.academia.edu/26166583/Influence_of_metal_surface_preparation_on_its_surface_profile_contact_angle_surface_energy_and_adhesion_with_glass_fibre_prepreg> [Accessed 18 April 2020].

iso.org. 2009. ISO 80000-1:2009 Quantities And Units — Part 1: General. [online] Available at: <https://www.iso.org/standard/30669.html> [Accessed 26 April 2020].

Jamieson, C., 2019. Why Your Old Five-Star NCAP Car Isn't As Safe As You Think It Is. [online] www.topgear.com. Available at: <https://www.topgear.com/car-news/crash/why-your-old-five-star-ncap-car-isnt-safe-you-think-it#3> [Accessed 10 April 2020].

L. Weirdie, B. and A. Lagace, P., 2007. ON THE USE OF QUASI-STATIC TESTING TO ASSESS IMPACT DAMAGE RESISTANCE OF COMPOSITE SHELL STRUCTURES. Journal Mechanics of Composite Materials and Structures, [online] 5(1), p.118. Available at: <https://www.tandfonline.com/doi/abs/10.1080/10759419808945895> [Accessed 10 April 2020].

Mamalis, A., Manolakos, D., Demosthenous, G. and Ioannidis, M. (1998). Crash worthiness of Composite Thin- Walled Structural Components. Boca Raton: CRC Press LLC, p.1.

Michele, G., 2018. Design validation of a composite crash absorber energy to an emergency landing. Advances in Aircraft and Spacecraft Science, [online] 5(3), p.333. Available at: <https://www.researchgate.net/publication/325466514_Design_validation_of_a_composite_crash_absorber_energy_to_an_emergency_landing> [Accessed 10 April 2020].

Milan, R., Viktor, K., Sergii, B. and Vit, S. (2014). Development of composite energy absorber. Procedia Engineering, [online] 96(1877-7058), p.393. Available at:

https://www.researchgate.net/publication/275540859_Development_of_Composite_Energy_Absor ber?enrichId=rgreq-24c7a4cf4195edbc26fadf916be5049cXXX&enrichSource=Y292ZXJQYWdlOzI3NTU0MDg1OTtBUzoyMzYyNzEwOTYyOTk1MjBAMTQzMzM0MjgyNzg1MQ%3D%3D&el=1_x_2&_esc=publicationCoverPdf [Accessed 10 April. 2020].

Motor-car.net. (n.d.). Space Frame Chassis. [online] Available at: https://motor-car.net/innovation/car-body/item/14795-space-frame [Accessed 10 April. 2020].

Nagra, D., n.d. Car Safety Features Explained. [online] www.which.co.uk. Available at: <https://www.which.co.uk/reviews/new-and-used-cars/article/car-safety-features-explained> [Accessed 13 April 2020].

Pollitt, C., 2019. LAMBORGHINI COUNTACH – WILD BULL. [online] www.carandclassic.co.uk. Available at: <https://www.carandclassic.co.uk/magazine/lamborghini-countach-wild-bull/> [Accessed 10 April 2020].

Santoni, P. 2015. Forum Post. 05/05/2015. Steel Chassis tube Spec On 339ountach. [Online]. [Accessed 10/04/20]. Available from: https://www.lamborghinichat.com/forum/threads/steel-chassis-tube-spec-on-countach.485503/.

shdcomposites.com. 2018. MTC510 Epoxy Component Prepreg. [online] Available at: <https://shdcomposites.com/admin/resources/mtc510-tds.pdf> [Accessed 16 April 2020].

Sheehan, S., 2016. Ultra-Lightweight Caterham Seven Uses Bicycle Frame Technology. [online] www.autocar.co.uk. Available at: <https://www.autocar.co.uk/car-news/new-cars/ultra-lightweight-caterham-seven-uses-bicycle-frame-technology> [Accessed 10 April 2020].

Steelconstruction.info. n.d. Member Design. [online] Available at: <https://www.steelconstruction.info/Member_design> [Accessed 16 April 2020].

steelnumber.com. n.d. E220 (1.0215). [online] Available at: <http://www.steelnumber.com/en/steel_composition_eu.php?name_id=565> [Accessed 16 April 2020].

Stibor, M., 2014. Buckling Reduction Factor Vs. Non-Dimensional Slenderness. [image] Available at: <https://structural-analyser.com/domains/SteelDesign/Buckling/> [Accessed 16 April 2020].

Sun, G., Li, S., Liu, Q., Li, G. and Li, Q., 2016. Experimental study on crashworthiness of empty/aluminum foam/honeycomb-filled CFRP tubes. Composite Structures, [online] 152, p.991. Available at: <https://www.sciencedirect.com/science/article/pii/S0263822316308467> [Accessed 10 April 2020].

supercarnostalgia.com. n.d. LAMBORGHINI COUNTACH LP500. [online] Available at: <https://supercarnostalgia.com/blog/lamborghini-countach-lp500> [Accessed 10 April 2020].

Suttie, A., 2013. Caterham Seven (K-Series) Buying Guide: Chassis. [online] www.pistonheads.com. Available at: <https://www.pistonheads.com/news/ph-buying-guide-contents/caterham-seven-k-series-buying-guide-chassis/28979> [Accessed 14 April 2020].

T. Bartlett Quimby, 2014. Global Vs. Local Buckling. [image] Available at: <https://www.bgstructuralengineering.com/BGSCM13/BGSCM006/index.htm> [Accessed 16 April 2020].

Taheri-Behrooz, F., Abdolvand, H. and Shokrieh, M. (2013). Designing and manufacturing of a drop weight impact test machine. Engineering Solid Mechanics 1, [online] p.69. Available at: https://www.researchgate.net/publication/270215383_Designing_and_manufacturing_of_a_drop_ weight_impact_test_machine [Accessed 10 April. 2020].

Webster, L., 2006. The Homemades. [online] www.caranddriver.com. Available at: <https://www.caranddriver.com/features/a15150678/the-homemades-feature/> [Accessed 13 April 2020].

Weernink, W. (2005). No crash test for 1,000s of new cars. [online] www.europe.autonews.com. Available at: https://europe.autonews.com/article/20051031/ANE/51102012/no-crash-test-for-1000s-of-new-cars [Accessed 10 April. 2020].

White, M. and Jones, N. (1999). Experimental quasi-static axial crushing of top-hat and double-hat thin-walled sections. International Journal of Mechanical Sciences, [online] 41, p.187. Available at: https://www.sciencedirect.com/science/article/pii/S0020740398000472 [Accessed 10 April. 2020].

Williams, T., Pennington, A. and Barton, D. (2000). The frontal impact response of a spaceframe chassis sportscar. Journal of Automobile Engineering, [online] 214(8), p.865. Available at: https://journals.sagepub.com/doi/abs/10.1177/095440700021400805 [Accessed 10 April. 2020].

Williams, T., Pennington, A. and Barton, D., 2000. The frontal impact response of a spaceframe chassis sportscar. Proceedings of the Institution of Mechanical Engineers, Part D: Journal of Automobile Engineering, [online] 214(8), p.1. Available at: <https://journals.sagepub.com/doi/abs/10.1177/095440700021400805> [Accessed 10 April 2020].

Yoon, J., Lee, Y. and Huh, H. (2013). Investigation of Deformation and Collapse Mechanism for Magnesium Tube in Axial Crushing Test. Journal of Mechanical Science and Technology, [online] 27(10), p.2918. Available at: https://www.researchgate.net/publication/271973021_Investigation_of_deformation_and_collapse _mechanism_for_magnesium_tube_in_axial_crushing_test [Accessed 10 April. 2020].

Appendices are available as 'supplementary files' (please see download area)